

CONTROL SYSTEM DESIGN FOR REDUCED THRUSTER-FLEXIBILITY INTERACTIONS IN SPACE ROBOTS

E. Martin

E. Papadopoulos

J. Angeles

Department of Mechanical Engineering and Centre for Intelligent Machines,
McGill University, Montreal, Quebec, Canada, H3A 2A7
emartin@cim.mcgill.ca, egpapado@cim.mcgill.ca, angeles@cim.mcgill.ca

ABSTRACT

Space manipulators mounted on an on-off thruster-controlled base are envisioned to assist in the assembly and maintenance of space structures. When handling large payloads, manipulator joint and link flexibility become important, for it can result in payload-attitude controller fuel-replenishing dynamic interactions. In this paper, the dynamic behaviour of a one-flexible-joint manipulator on a free-flying base is studied, while its parameters are matched with available space-manipulator data. Describing functions are used to predict the dynamic performance of two alternative controller/estimator schemes, and to conduct a parametric study on the influence of key system parameters. Design guidelines and a particular state-estimator are suggested that can minimize such undesirable dynamic interactions as well as thruster fuel consumption.

1. INTRODUCTION

Robotic devices in orbit will play an important role in space exploration and exploitation. The mobility of such devices can be enhanced by mounting them on free-flying bases, controlled by on-off thrusters. Such robots introduce a host of dynamic and control problems not found in terrestrial applications. When handling large payloads, manipulator joint or structural flexibility becomes important and can result in payload-attitude controller fuel-replenishing dynamic interactions. Such interactions may lead to control system instabilities, or manifest themselves as limit cycles [1].

The CANADARM-Space Shuttle system is the only operational space robotic system. Its Reaction Control System (RCS), which makes use

of on-off thrusters, is designed using single-axis, rigid-body motion, and a thruster switching logic based on phase-plane techniques. This approach is common in the design of thruster-based control systems. The flexible modes of this space robotic system have rather low frequencies, which continuously change with manipulator configuration and payload, and can be excited by the RCS activity. The performance degradation of the RCS due to the deployment of a *flexible payload*, with or without the CANADARM, was studied in [2]. A new design for the RCS was developed to reduce the impact of large measurement uncertainties in the rate signal during attitude control, as reported in [3]. The performance of the RCS is increased significantly for rigid-body motion. However, the flexibility problem was not addressed. Currently, the method for resolving these problems consists of performing extensive simulations. If dynamic interactions occur, corrective actions are taken, which would include adjusting the RCS parameter values, or simply changing the operational procedures [2]. The consequences of such interactions can be problematic, since fuel is an unavailable resource in space; hence, classical attitude controllers must be improved to reduce the possibility of such dynamic interactions.

This problem was studied using a single mode, linear translational mechanical system to approximate the dynamic behavior of a two-flexible joint manipulator mounted on a three-degrees-of-freedom (dof) base [4]. A particular state-estimator model and design guidelines were suggested to minimize such undesirable dynamic interactions, as well as thruster fuel consumption. In this paper, these results are validated using a more realistic model with rotational dof. A general technique to model a space manipulator with

flexible joints is first developed and used to derive the dynamics of a planar system consisting of a single-flexible-joint manipulator on a three-dof spacecraft. The describing function technique and simulations are used to study this four-dof system and show the increase in performance that can be obtained using the state-estimator model developed in [4]. Design guidelines for such systems are also presented.

2. SYSTEM DESCRIPTION

Dynamics Modelling

In this section, the dynamic model of an N -flexible-joint space manipulator is obtained using a Lagrangian approach. Since the travel of the system is assumed to be relatively short in length and duration, the dynamical effects due to orbital mechanics are neglected. The kinematics of the free-flying space manipulator is expressed using the spacecraft centre of mass (CM) C as a reference point to describe the translation of the system. The inertial position vector of an arbitrary point P of the system, \mathbf{p} , can be written as

$$\mathbf{p} = \mathbf{c} + \boldsymbol{\rho} \quad (1)$$

where \mathbf{c} is the position vector of C and $\boldsymbol{\rho}$ is the position vector of point P with respect to C , as shown in Fig. 1. The position vector $\boldsymbol{\rho}$ can be further expressed as

$$\boldsymbol{\rho} = \mathbf{c}_i + \mathbf{p}_i \quad (2)$$

where \mathbf{c}_i is the position vector of the CM C_i of the i -th body with respect to the spacecraft CM, and \mathbf{p}_i is the position vector of point P with respect to the i -th body CM. The position vector \mathbf{c}_i can be expressed as

$$\mathbf{c}_i = \mathbf{r}_0 + \sum_{k=1}^{i-1} (\mathbf{r}_k - \mathbf{l}_k) - \mathbf{l}_i, \quad i = 1, \dots, N \quad (3)$$

with vectors $\{\mathbf{r}_k\}_0^{i-1}$ and $\{\mathbf{l}_k\}_1^i$ indicated in Fig. 1. The velocity of the point P on the manipulator is expressed as

$$\dot{\mathbf{p}} = \dot{\mathbf{c}} + \dot{\mathbf{c}}_i + \boldsymbol{\omega}_i \times \mathbf{p}_i \quad (4)$$

with

$$\dot{\mathbf{c}}_i = \boldsymbol{\omega}_0 \times \mathbf{r}_0 + \sum_{k=1}^{i-1} \boldsymbol{\omega}_k \times (\mathbf{r}_k - \mathbf{l}_k) - \boldsymbol{\omega}_i \times \mathbf{l}_i \quad (5)$$

where $\boldsymbol{\omega}_0$ is the angular velocity of the spacecraft, and $\boldsymbol{\omega}_i$ is the angular velocity of the coordinate frame attached to the i -th link of the manipulator, which can be expressed as

$$\boldsymbol{\omega}_i = \boldsymbol{\omega}_0 + \sum_{k=1}^i \dot{\theta}_{2k} \mathbf{z}_k \quad (6)$$

where $\dot{\theta}_{2k}$ is the joint rate of the k -th joint and \mathbf{z}_k is the unit vector along the axis of rotation of the same joint, see Fig. 2.

By choosing a set of Euler angles $\boldsymbol{\delta}$ to describe the attitude of the base, its angular velocity $\boldsymbol{\omega}_0$ can then be expressed in terms of the Euler rates $\dot{\boldsymbol{\delta}}$ as [5]

$$\boldsymbol{\omega}_0 = \mathbf{S}_0(\boldsymbol{\delta}) \dot{\boldsymbol{\delta}} \quad (7)$$

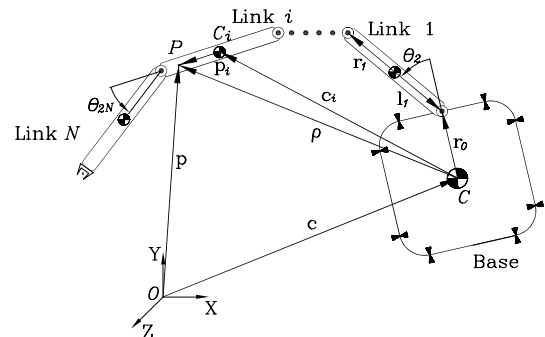


Figure 1: A space manipulator system.

Assuming lumped flexibility at the joints, links are considered rigid and Eqs.(4) and (5) can be substituted in the kinetic energy expression of the manipulator, given by

$$T_M = \frac{1}{2} \int_M \dot{\mathbf{p}}^T \dot{\mathbf{p}} dM = T_0 + T_1 + T_2 \quad (8)$$

where M is the total mass of the system, and T_0 , T_1 , and T_2 are defined as

$$T_0 = \frac{1}{2} M (\dot{\mathbf{c}}^T \dot{\mathbf{c}}), \quad T_1 = \dot{\mathbf{c}}^T \left(\sum_{i=1}^N m_i \dot{\mathbf{c}}_i \right)$$

$$T_2 = \frac{1}{2} \left[\boldsymbol{\omega}_0^T \mathbf{I}_0 \boldsymbol{\omega}_0 + \sum_{i=1}^N (m_i \dot{\mathbf{c}}_i^T \dot{\mathbf{c}}_i + \boldsymbol{\omega}_i^T \mathbf{I}_i \boldsymbol{\omega}_i) \right]$$

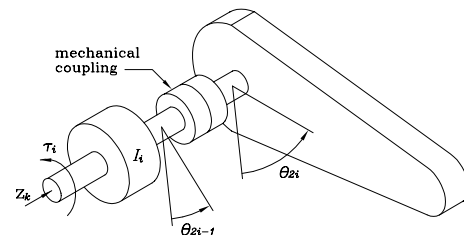


Figure 2: A flexible-joint model.

with m_i and I_i being the i -th body mass and moment of inertia with respect to the centre of mass of the corresponding body.

Now, assuming direct drives, see Fig. 2, and defining $\boldsymbol{\theta}_m = [\theta_1, \theta_3, \dots, \theta_{2N-1}]^T$ as the vector of the rotor-joint variables, at the joints, the kinetic energy of the rotors is

$$T_m = \frac{1}{2} \dot{\boldsymbol{\theta}}_m^T \mathbf{J} \dot{\boldsymbol{\theta}}_m \quad (9)$$

where \mathbf{J} is the rotors moment of inertia matrix.

For a free-flyer, microgravity effects are very small compared to control forces, and hence, they are neglected. Thus, the potential energy is only due to joint elasticity, and can be written as

$$V = \frac{1}{2} \Delta \boldsymbol{\theta}^T \mathbf{K} \Delta \boldsymbol{\theta} \quad (10)$$

where \mathbf{K} is a stiffness matrix and $\Delta \boldsymbol{\theta}$ a vector representing the difference between the angular position of the link and the angular position of the rotor, its i th component being $\theta_{2i} - \theta_{2i-1}$.

Viscous friction forces due to damping can be taken into account using Rayleigh's dissipation function R , given by

$$R = \frac{1}{2} \Delta \dot{\boldsymbol{\theta}}^T \mathbf{C} \Delta \dot{\boldsymbol{\theta}} \quad (11)$$

where \mathbf{C} is a damping matrix.

The sum of all powers developed by driving devices supplying controlled forces is given by

$$\Pi = \boldsymbol{\tau}^T \dot{\boldsymbol{\theta}}_m + \mathbf{f}^T \dot{\mathbf{c}} + \mathbf{n}^T \boldsymbol{\omega}_0 \quad (12)$$

where $\boldsymbol{\tau}$ is the vector containing all torques applied by the motors at each joints, while \mathbf{f} and \mathbf{n} are the forces and moments applied to the spacecraft with devices like thrusters and/or momentum wheels. Note that if vector \mathbf{c} is expressed in the inertial frame, \mathbf{f} must be expressed in the same frame. If \mathbf{t} denotes the thruster forces expressed in the spacecraft frame, then \mathbf{f} can be written as

$$\mathbf{f} = \mathbf{R}(\boldsymbol{\delta}) \mathbf{t} \quad (13)$$

where $\mathbf{R}(\boldsymbol{\delta})$ is a rotation matrix carrying the inertial frame into an orientation identical to that of the spacecraft frame. Therefore, using Eqs.(7) and (13), Eq.(12) becomes

$$\Pi = \boldsymbol{\tau}^T \dot{\boldsymbol{\theta}}_m + (\mathbf{R}\mathbf{t})^T \dot{\mathbf{c}} + \mathbf{n}^T \mathbf{S}_0 \dot{\boldsymbol{\delta}} \quad (14)$$

In the realm of the Euler-Lagrange equations, we use $\mathbf{q} = [\mathbf{c}^T, \boldsymbol{\delta}^T, \boldsymbol{\theta}^T]^T$, where $\boldsymbol{\theta}$ is the vector of

the joint angles of both the rotors and the links, which are different due to flexibility, and all other quantities have been defined in Eqs.(1) and (7). Then, applying Euler-Lagrange equations

$$\frac{d}{dt} \left(\frac{\partial T}{\partial \dot{q}_i} \right) - \frac{\partial T}{\partial q_i} + \frac{\partial V}{\partial q_i} = \frac{\partial}{\partial \dot{q}_i} (\Pi - R) \quad (15)$$

for $i = 1, \dots, 6 + 2N$, the equation of motion can be written as

$$\mathbf{M} \ddot{\mathbf{q}} + \mathbf{C}_2 \dot{\mathbf{q}} + \mathbf{K}_2 \mathbf{q} + \mathbf{n} = \boldsymbol{\phi} \quad (16)$$

where \mathbf{M} is a $(6 + 2N) \times (6 + 2N)$ positive-definite mass matrix, \mathbf{C}_2 , \mathbf{K}_2 and \mathbf{n} containing the damping coefficient terms, the stiffness terms and the nonlinear velocity terms respectively, while $\boldsymbol{\phi}$ is the vector of generalized forces.

Controller Structure

The technology currently available does not allow the use of proportional thruster valves in space, and thus, the classical PD and PID control laws cannot be used. Therefore, spacecraft attitude and position are controlled by the use of on-off thruster valves, that introduce nonlinearities.

The usual scheme to control a spacecraft with on-off thrusters is by the use of the error phase plane, defined as having the spacecraft attitude error e and error rate \dot{e} as coordinates. The on-and-off switching is determined by switching lines in the phase plane and can become complex, as for example, the phase plane controller of the Space Shuttle [2]. To simplify the switching logic, two switching lines with equations $e + \lambda \dot{e} = \pm \delta$ have been used, as shown in Fig. 3. The deadband limits $[-\delta, \delta]$ are determined by attitude limit requirements, while the slope of the switching lines, by the desired rate of convergence towards the equilibrium and by the rate limits. This switching logic can be represented as a relay with a deadband, where the input is $e + \lambda \dot{e}$, the left-hand side of the switching-line equations, see Fig. 4.

To compute the input to the controller, the position and the velocity of the base are required. Using current space technology, both states can be obtained from sensors. However, it can happen that only the attitude is available and then, the angular velocity must be estimated.

3. SIMPLIFIED SYSTEM

In this section, the equations of motion of a simplified system are developed using the modelling

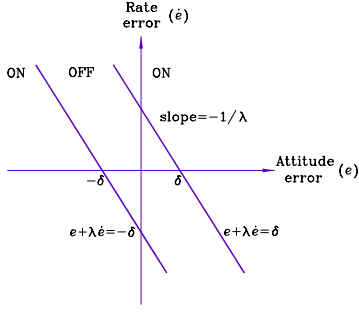


Figure 3: Switching logic in the error phase plane.

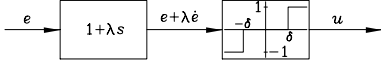


Figure 4: Controller block.

techniques presented in Section 2. Here, we consider the planar-one-flexible-joint manipulator on the 3-dof spacecraft of Fig. 5. We assume that only on-off thrusters are available to control the attitude of the spacecraft, and that the moments produced are either 0, n_{max} or $-n_{max}$. Moreover, we assume that no control on the local x_0 and y_0 direction of the spacecraft is exerted.

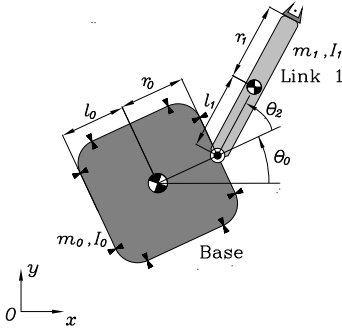


Figure 5: A planar free-flying manipulator.

If we assume that the joint is braked in a specific configuration θ_1 , then the vector of generalized coordinates is $\mathbf{q} = [x_s, y_s, \theta_0, \theta_2]^T$, where x_s and y_s are the spacecraft CM coordinates with respect to an inertial frame, θ_0 is the spacecraft attitude, and θ_2 is the angular position of link 1. Applying the techniques of Section 2, the equations of motion are obtained as

$$-c\dot{\theta}_2 + k\theta_1 - k\theta_2 = \tau_1 \quad (17a)$$

$$\mathbf{M}(\mathbf{q})\ddot{\mathbf{q}} + \mathbf{C}\dot{\mathbf{q}} + \mathbf{K}\mathbf{q} + \mathbf{n} = \boldsymbol{\phi} \quad (17b)$$

where all matrices are of 4×4 and all vectors are 4-dimensional. Moreover,

$$\mathbf{C} = \text{diag}(0 \ 0 \ 0 \ c), \quad \mathbf{K} = \text{diag}(0 \ 0 \ 0 \ k),$$

$$\boldsymbol{\phi} = [0, 0, n, k\theta_1]^T$$

with the components M_{ij} of \mathbf{M} and n_i of \mathbf{n} being given in the Appendix.

Equation (17a) gives the expression for the torque required to brake the joint, and Eq.(17b) represents the dynamics of the system. This equation can be linearized about an operating point. For example, the point $\theta_0 = \theta_0^* = \text{const.}$, and $\theta_2^* = \theta_1^* = \text{const.}$ Defining $\delta\mathbf{q} = [\delta x_s, \delta y_s, \delta\theta_0, \delta\theta_1]^T$, where $\delta\theta_0 = \theta_0 - \theta_0^*$ and $\delta\theta_1 = \theta_2 - \theta_1^*$, the linearized equations can be written as

$$\mathbf{M}(\theta_0^*, \theta_1^*)\delta\ddot{\mathbf{q}} + \mathbf{C}\delta\dot{\mathbf{q}} + \mathbf{K}\delta\mathbf{q} = \boldsymbol{\phi}_l \quad (18)$$

where \mathbf{M} , \mathbf{C} and \mathbf{K} were already defined in Eq.(17) and $\boldsymbol{\phi}_l$ is now given by

$$\boldsymbol{\phi}_l = [0, 0, n, 0]^T \quad (19)$$

The natural frequencies of this system are simply given by the square roots of the eigenvalues of the dynamic matrix \mathbf{W} , which is defined as

$$\mathbf{W} \equiv \mathbf{M}(\theta_0^*, \theta_1^*)^{-1}\mathbf{K} \quad (20)$$

with $\mathbf{M}(\theta_0^*, \theta_1^*)$ being a positive-definite matrix, and hence, nonsingular. Moreover, three eigenvalues are zero and correspond to spacecraft rigid modes, while the fourth one corresponds to joint flexibility.

Note that a payload can be added at the end of the link without any modification of the previous dynamic model. The parameters of the link, m_1 , I_1 , r_1 and l_1 , just have to be adjusted accordingly. We can also define the parameter β as the ratio of the mass of the payload over the mass of the base, $\beta = m_p/m_0$, where m_p is the mass of the payload. It is also useful to define the parameter γ as the angular acceleration of the spacecraft, $\gamma = n/I_{t_0}$, where I_{t_0} is the moment of inertia of the whole system about the spacecraft CM. Finally, we define γ_0 as the nominal angular acceleration of the spacecraft itself, i.e., $\gamma_0 = n/I_0$.

4. CONTROL AND ANALYSIS

Frequency-Domain Analysis

Since the attitude controller assumes use of on-off thrusters, which are nonlinear devices, the system cannot be adequately analyzed through the application of linear analysis methods. This problem is solved using the describing-function method, which can predict the existence of limit cycles in nonlinear systems [6, 7].

In order to use this method, the system under study must be partitioned into a linear and a nonlinear part. Then, it is transformed into the configuration shown in Fig. 6. $G(j\omega)$ is the frequency response of all the linear elements in the system and $N(A, \omega)$ is the describing function of the non-linearity, which is tabulated in many books, e.g., in [7]. The reader is referred to [6] and [7] for a detailed description of the method, and to [4] for the application of this method to the problem at hand. The same stability definition derived in [4] is used in this paper, and is reproduced here.

Stability Definition

1. **Unstable system.** This is either a system whose motion diverges or a system whose motion reaches a limit cycle that is not contained inside the switching lines as for a rigid body limit cycle, thus resulting in a large rate of fuel consumption;
2. **Stable system.** This is a system whose motion reaches an unavoidable limit cycle similar to a rigid-body limit cycle, thus being contained between the switching lines, and resulting in a near-zero rate of fuel consumption, as for a rigid system.

For the simplified system at hand, the dynamics of the plant is nonlinear. However, it is still possible to use the linearized model of the plant and obtain the transfer function that relates the moment n applied to the spacecraft, to its attitude θ_0 . Note that this transfer function is independent of the attitude of the spacecraft since, in space, the system behaviour is exactly the same, whatever the attitude is. It was thus possible to transfer our system into the configuration of Fig. 6.

Control Laws

As stated in Section 2, the attitude and its rate are required to compute the input to the controller. However, it may happen that only the

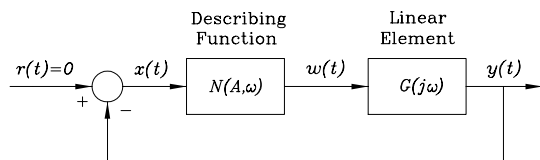


Figure 6: A feedback system whose nonlinear part has been replaced by its corresponding describing function.

attitude is available and thus, a state estimator must be used to obtain the required velocity. As shown in [4], the use of sensors to obtain the rate of the base may deteriorate the performance of the system due to the high-frequency filtering requirements. Here, we consider that only the attitude is available from sensors, and, hence, to obtain the velocity, we use two different state estimators.

In Case 1, a controller-plant-estimator configuration similar to the one used on the Space Shuttle is employed [2]. The plant is described by its nonlinear model for simulations, while its linearized model is used for describing-function purposes. A differentiator combined with a second-order filter is used to obtain a velocity estimate, as shown in Fig. 7. The differentiation of a noisy signal is usually not recommended because it amplifies noise. However, in this case, it is possible to use a scheme where only the flexible part of the motion needs to be differentiated. This means that, at the limit, for a rigid system, no differentiation is necessary. This state estimator can give very good results when flexibility is low. The differentiator-filter is given by $sG_{se}(s)$ where

$$G_{se}(s) = \frac{\omega_{se}^2}{s^2 + 2\zeta_{se}\omega_{se}s + \omega_{se}^2} \quad (21)$$

The attitude feedback is also low-pass-filtered using a second-order filter represented by the transfer function $G_f(s)$, namely,

$$G_f(s) = \frac{\omega_f^2}{s^2 + 2\zeta_f\omega_f s + \omega_f^2} \quad (22)$$

For this filter, we use $\zeta_f = 0.707$, and let ω_f free to vary, while, for the differentiator-filter, we use values that correspond to the ones used on the Space Shuttle [2], namely, $\omega_{se} = 0.2513$ rad/s and $\zeta_{se} = 0.707$

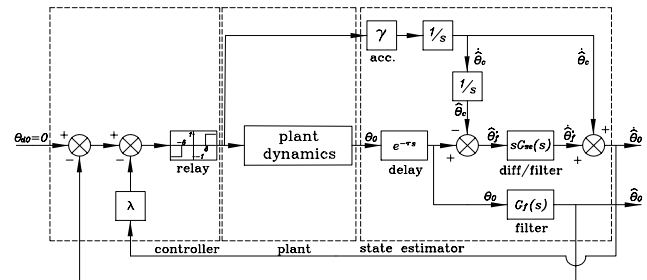


Figure 7: Case 1: model with a velocity estimator and a position filter.

For Case 2, an asymptotic state observer is used to obtain an estimate for the attitude and its rate

from an attitude measurement [8]. The configuration corresponding to this case is depicted in Fig. 8. The estimator, which is model-based, is built using the linearized model of the plant, written in state-space form, namely,

$$\begin{aligned}\dot{\mathbf{x}} &= \mathbf{A}\mathbf{x} + \mathbf{b}u \\ \mathbf{y} &= \mathbf{C}\mathbf{x}\end{aligned}$$

However, for simulation purposes, the plant is described by its full nonlinear model. To be observable, the x_s and y_s positions of the spacecraft and its attitude θ_0 must be available for feedback in the estimator. Therefore, the gain matrix \mathbf{L} , as shown in Fig. 8, is of 8×3 and thus, 24 gains must be determined. Multiple solutions are possible, of which we choose the one implemented in *Matlab*, which makes use of the algorithm presented in [9]. The 8 pole locations are those of the Butterworth filter at the chosen frequency ω_f [10].

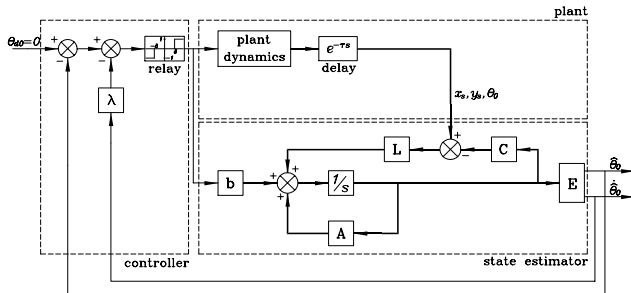


Figure 8: Case 2: model with an asymp. st. est.

In these two cases, a time delay τ , see Figs. 7 and 8, has been included to account for the delay between the time a sensor reads a measurement, and the time this measurement is used. Since this delay is more significant than the delay of turning on or off the thrusters, only a sensor time delay is included.

Parametric Studies and Results

The frequency expression of Eq.(20) was used to obtain the required spring stiffness k and damping coefficient c of the flexible joint such that the first natural frequency of the Space Shuttle/CANADARM system was matched for a specific configuration, without payload. Using the system parameter values of Table 1 [11], where $x_c = (2712 + 15.5\beta m_0)/(320 + \beta m_0)$, the required k and c were found to be

$$k = 123,985 \text{ Nm/rad} \quad (23)$$

$$c = 6,166 \text{ Nms/rad} \quad (24)$$

for the CANADARM in a configuration that corresponds to the one of Fig. 5, with $\theta_1 = \theta_2 = 45$ deg. In this configuration, its first natural frequency is $\omega_n = 2\pi(0.32)$ rad/s, and the damping ratio is $\zeta = 0.05$, without payload.

Using the describing function method, a parametric study was undertaken to investigate the significance of key system parameters. The two cases presented above are analyzed using the fixed parameter values of Table 2, and the range of parameter values of Table 3, both being based on available space manipulator data [11].

The results of the parametric study for Case 1 are illustrated with the use of stability maps, as those depicted in Fig. 9. Figure 9(a) shows the stability boundary for different cutoff frequencies ω_f of the second-order filter $G_f(s)$ given by Eq.(22). The region below such boundary represents a zone where the system is stable, while the region above corresponds to a zone of instability. As shown in the same figure, the stability zone can be increased by increasing the cutoff frequency ω_f . Analyzing the graphs in Fig. 9 in a similar way, guidelines for the design of attitude control systems when flexibility is a major concern, are obtained as follows:

1. The cutoff frequency ω_f for the filters should be chosen as large as possible to avoid instability;
2. the velocity gain λ should be chosen with care since the system can be unstable for low and high velocity gain values;
3. the acceleration of the base γ_0 should be kept small for stability. Unstable types of behavior are more likely to occur for large γ_0 ;
4. deadband limits δ should be chosen as large as possible to avoid instability.

Table 2: Fixed-parameter values.

τ (s)	ω_{se} (rad/s)	ζ_f	ζ_{se}
0.1	0.2513	0.707	0.707

Table 3: Free-parameter values.

β	$0.01 \leq \beta \leq 0.3$
λ (s)	$0.1 \leq \lambda \leq 50$
γ_0 (deg/s ²)	$0.002 \leq \gamma_0 \leq 2$
δ (deg)	$0.1 \leq \delta \leq 20$
θ_1	$0^\circ, 45^\circ, 90^\circ, 135^\circ, 180^\circ$
ω_f (rad/s)	$0.2513 \leq \omega_f \leq 20$

Table 1: Shuttle, simplified 1-link manipulator and payload parameter values.

Body	l_i (m)	r_i (m)	m_i (kg)	I_i (kg m ²)
0		1	75,000	1,635,937
1	x_c	$15.5 - x_c$	$320 + \beta m_0$	$(320 + \beta m_0)x_c^2 - (5423.5 + 31\beta m_0)x_c + 31424.11 + 240.25\beta m_0$

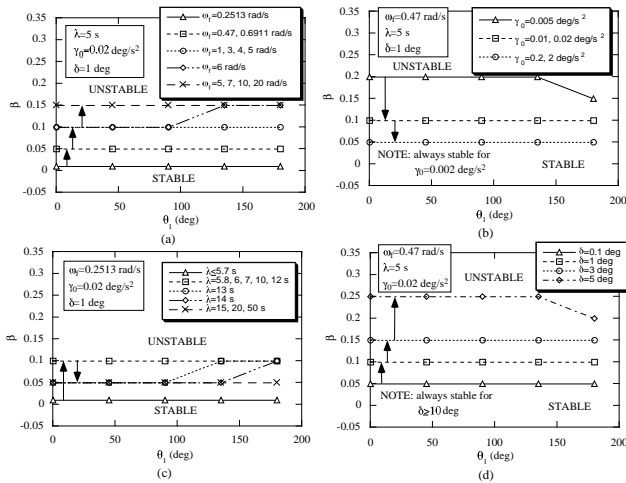


Figure 9: Describing function stability maps for Case 1 showing: (a) the effect of the cutoff frequency ω_f ; (b) the effect of the base acceleration γ_0 ; (c) the effect of the velocity gain λ ; and (d) the effect of the deadband limit δ .

The upper limits of these parameters are set by design requirements or available hardware.

The model corresponding to Case 1 (Fig. 7) was simulated using the parameters in Tables 2 and 4. Simulation results for an initial base angular error of 0.05 rad are shown in Fig. 10. Figures 10(b) and (c) show that thrusters are firing continuously, thus resulting in a high total fuel consumption of 1672.2 fuel units, and a large rate of fuel consumption. Therefore, the system is classified as unstable. Moreover, the phase-plane trajectories in Fig. 10(a), show that a large limit cycle is reached due to the dynamic interactions.

However, using the system configuration of Case 2, shown in Fig. 8, with the same parameters, provides very interesting results, as shown in Fig. 11. From Figs. 11(a) and (b), it can be seen that a limit cycle contained between the switching lines is reached, which leads to a stable system. Figures 11(c) and (d) are also typical of a stable system, since the thrusters are not firing

Table 4: Free-parameter values for simulations.

β	λ (s)	γ_0	δ	θ_1	ω_f (rad/s)
.25	10	$0.02^\circ/s^2$	1°	135°	0.2513

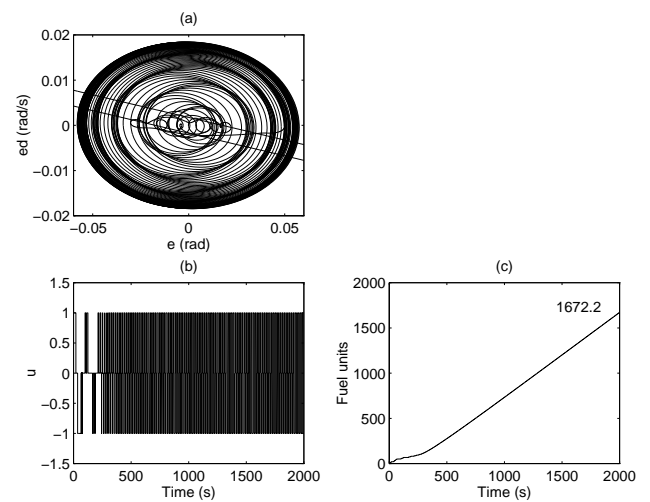


Figure 10: Simulation results for Case 1: (a) Spacecraft error phase plane; (b) Thruster command history; and (c) Fuel consumption.

continuously and the fuel-consumption curve is flat, thereby resulting in a near-zero rate of fuel consumption, similar to that for a rigid body system. In this case, the total fuel consumption is very small compared to Case 1, namely, 39.7 fuel units only. Therefore, it is observed that the use of the proposed state estimator increases the performance of the control system significantly, and extends the system operational life. In addition, using the describing function method, it can be shown that this estimator results in a system that is almost always stable for the whole range of parameters, thus resulting in significantly increased stability margins in comparison to Case 1.

5. CONCLUSIONS

This work examined the dynamic interactions between the attitude controller of a spacecraft and the flexible modes of a space manipulator mounted on it. A general technique to model the dynamics of a space manipulator with flexible joints was developed, and a simple planar model was used to analyze two different control/estimation schemes with the describing-function method. Guidelines for the design of such systems were produced. This study also showed that the use of an asymptotic state esti-

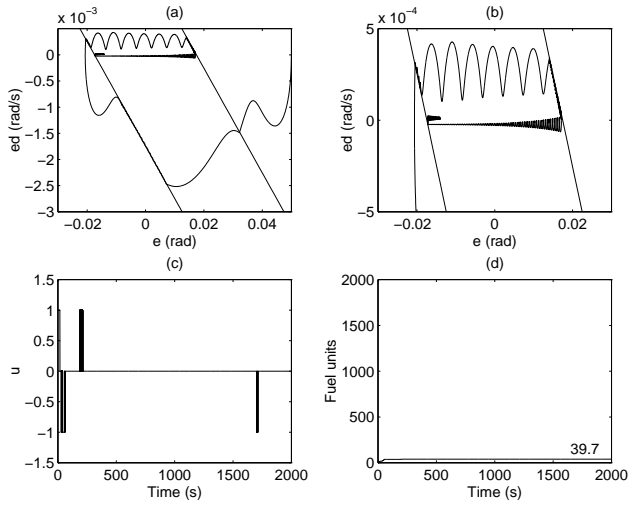


Figure 11: Simulation results for Case 2: (a) Spacecraft error phase plane; (b) Spacecraft error phase plane (zoom); (c) Thruster command history; and (d) Fuel consumption.

mator improves significantly the stability and the performance of the system.

ACKNOWLEDGEMENTS

The support of this work by the Fonds pour la Formation de Chercheurs et l'Aide à la Recherche (FCAR), and by the Natural Sciences and Engineering Council of Canada (NSERC) is gratefully acknowledged. The first author is an NSERC Class-of-67 Scholar.

REFERENCES

- [1] R.A. Millar and F.R. Vigneron, 1979, "Attitude Stability of a Pseudorate Jet-Controlled Flexible Spacecraft," *J. of Guid., Cont., and Dyn.*, 2(2), pp. 111–118.
- [2] L.L. Sackett and C.B. Kirchwey, 1982, "Dynamic Interaction of the Shuttle On-Orbit Flight Control System with Deployed Flexible Payload," *Proc. of the AIAA Guid. and Cont. Conf.*, San Diego, CA, pp. 232–245.
- [3] E.T. Kubiak and M.W. Martin, 1983, "Minimum Impulse Limit Cycle Design to Compensate for Measurement Uncertainties," *J. of Guid., Cont., and Dyn.*, 6(6), pp. 432–435.
- [4] E. Martin, E. Papadopoulos and J. Angeles, 1995, "On the Interaction of Flexible Modes and On-off Thrusters in Space Robotic Systems," *Proc. of the 1995 Int. Conf. on Intel-*

ligent Robots and Systems, IROS'95, Vol. 2, Pittsburgh, PA, pp. 65–70.

- [5] L. Meirovitch, 1970, *Methods of Analytical Dynamics*, McGraw-Hill.
- [6] J.-J.E. Slotine and W. Li, 1991, *Applied Nonlinear Control*, Prentice Hall, N.J.
- [7] D.P. Atherton, 1975, *Nonlinear Control Engineering*, Van Nostrand, New York.
- [8] C.T. Chen, 1984, *Linear System Theory and Design*, Holt, Rinehart, and Winston, N.Y.
- [9] J. Kautsky, N.K. Nichols and P. Van Dooren, 1985, "Robust Pole Assignment in Linear State Feedback," *Int. J. Cont.*, 41(5), pp. 1129–1155.
- [10] L.P. Huelsman, 1993, *Active and Passive Analog Filter Design*, McGraw-Hill.
- [11] E. Martin, 1994, "Interaction of Payload and Attitude Controller in Space Robotic Systems," Master Thesis, Dept. of Mech. Eng., McGill University, Montreal, Canada.

APPENDIX

The M_{ij} entries of \mathbf{M} in eq.(17) are given by

$$\begin{aligned}
M_{11} &= m_0 + m_1 \\
M_{12} &= 0 \\
M_{13} &= -m_1 r_0 \sin \theta_0 - m_1 l_1 \sin(\theta_0 + \theta_2) \\
M_{14} &= -m_1 l_1 \sin(\theta_0 + \theta_2) \\
M_{22} &= m_0 + m_1 \\
M_{23} &= m_1 r_0 \cos \theta_0 + m_1 l_1 \cos(\theta_0 + \theta_2) \\
M_{24} &= m_1 l_1 \cos(\theta_0 + \theta_2) \\
M_{33} &= I_0 + I_1 + m_1 r_0^2 + m_1 l_1^2 + 2m_1 r_0 l_1 \cos \theta_2 \\
M_{34} &= I_1 + m_1 l_1^2 + m_1 r_0 l_1 \cos \theta_2 \\
M_{44} &= I_1 + m_1 l_1^2
\end{aligned} \tag{25}$$

and the elements of \mathbf{n} in eq.(17) are given by

$$\begin{aligned}
n_1 &= -[m_1 r_0 \cos \theta_0 + m_1 l_1 \cos(\theta_0 + \theta_2)]\dot{\theta}_0^2 \\
&\quad - 2m_1 l_1 \cos(\theta_0 + \theta_2)\dot{\theta}_0 \dot{\theta}_2 \\
&\quad - m_1 l_1 \cos(\theta_0 + \theta_2)\dot{\theta}_2^2 \\
n_2 &= -[m_1 r_0 \sin \theta_0 + m_1 l_1 \sin(\theta_0 + \theta_2)]\dot{\theta}_0^2 \\
&\quad - 2m_1 l_1 \sin(\theta_0 + \theta_2)\dot{\theta}_0 \dot{\theta}_2 \\
&\quad - m_1 l_1 \sin(\theta_0 + \theta_2)\dot{\theta}_2^2 \\
n_3 &= -m_1 r_0 l_1 \sin \theta_2 \dot{\theta}_2^2 - 2m_1 r_0 l_1 \sin \theta_2 \dot{\theta}_0 \dot{\theta}_2 \\
n_4 &= m_1 r_0 l_1 \sin \theta_2 \dot{\theta}_0^2
\end{aligned} \tag{26}$$